EFFECT OF ALLOY COMPOSITION AND AGING ON THE SURVIVABILITY OF LEADFREE SOLDERS IN HIGH TEMPERATURE VIBRATION IN AUTOMOTIVE ENVIRIONMENTS

Pradeep Lall, Ph.D., MBA, Vikas Yadav, Di Zhang
Auburn University
NSF-CAVE3 Electronics Research Center and Department of Mechanical Engineering
Auburn, AL, USA
lall@auburn.edu

Robert Kinyanjui, Ph.D., Brad Palmer, Jesse Jangula
John Deere Electronic Solutions, Inc.
Fargo, ND, USA

ABSTRACT

Electronics in modern automotive platforms are being used to facilitate a number of operational and safety functions including energy generation, transmission, collision avoidance systems, lane departure warning systems, anti-lock braking systems, vehicle stability assist, global positioning, navigation and drive assist systems. During operation, automotive electronics in underhood environments may be simultaneously exposed to high temperatures in the neighborhood of 150-200°C in addition to vibration over a sustained period of time. Typical failure modes may include solder fatigue, copper trace or lead fracture. In prior studies, SnAgCu solders which are increasingly used in automotive electronics have shown susceptibility to evolution of the material properties under exposure to high temperature. However, the reliability of the solder alloys under combined exposure to vibration at high automotive temperatures is not well understood to a level which will allow the development of models for life-prediction. In this study a variety of packaging architectures fabricated with SAC105 and SAC305 alloys have been studied under exposure to random vibration and range of temperatures in the neighborhood of 25-125°C. Spectral content of the printed circuit board assemblies has been studied using accelerometer output. All the parts on the board assemblies have been monitored for resistive opens using a high-speed data-acquisition system. FE simulation using global-local finite element models is thus correlated with the system characteristics such as modal shapes, natural frequencies and displacement amplitudes for every temperature. The solder level stresses have been extracted from the sub-models. Stress amplitude versus cycles to failure curves are obtained at all the three test temperatures. A temperature and vibration-amplitude dependent-version of the Basquin power law damage relationship has been developed using the test data. Material properties of the PCB at test temperatures have been measured using tensile tests and dynamic mechanical analysis. A comparison of failure modes for different packaging architectures at elevated test temperatures and vibration has been presented in this study.

Key words: Leadfree solders, solder joint reliability, temperature-vibration, life-prediction models, acceleration factors, and automotive electronics

INTRODUCTION

Accelerated test data and modeling methods for assessment of reliability of leadfree electronics assemblies under simultaneous exposure to vibration and temperature is sparse. Prior studies on the loads encountered in automotive operation have revealed continuous maximum temperatures up to 140°C and vibration levels of up to 10g RMS [Johnson 2004]. The loads are even more consequential for the off-road automotives including construction and agricultural machinery where the vibration levels may be significantly higher than for on-road vehicles [Barker 1990, 1992, Basaran 2002, Qi 2004]. Modeling methods exist for reliability assessment of solder interconnects subjected to single stresses of vibration or under exposure to high temperature [Steinberg 1988, Henderson 1995, Hu 1995, Wong 1997, Lall 2005, Lall 2007]. Researchers have developed the theory and life prediction models for solder fatigue subjected to thermal cycling [Tavernelli 1962]. Similarly, the theory for life prediction and accelerated testing under random vibration is also well formalized for leaded solders [Steinberg 1988, Hu 1995, Henderson et al 1995]. Prior studies on the effect of concurrent thermal cycling and dynamic loading on electronic components have suggested incremental damage superposition approach for predicting solder joint reliability [Barker 1990, 1992, Basaran 2002, Qi 2004]. The behavior of 63Sn/37Pb solder under in-plane vibration at high temperature has been studied [Zhao 2000].

However, none of the prior work explicitly includes the temperature term in the combination with vibration-level in a closed-form damage prediction relationship to allow for life prediction under the action of simultaneous exposure to

vibration and temperature. In this paper, the authors have characterized the high cycle fatigue S-N curves of widely used SAC105 and SAC305 lead-free solders at various temperatures in the range expected during automotive underhood operation. In this paper, two test vehicles with SAC105, and SAC305 daisy chained CABGA, PBGA, QFP, SOP and TSOPs components have been tested to failure by subjecting the assemblies to elevated test temperatures and harmonic vibration levels at its first natural frequency of the board assembly. The test matrix includes different test temperatures and harmonic vibration amplitudes of 10g and 14g. Test vehicle-1 is tested at 10g stress level at operating temperatures of 25°C, 75°C and 125°C. Test vehicle-2 is tested at 14g stress level at operating temperatures of 25°C, and 55°C. In addition to pristine assemblies, the effect of isothermal aging has been studied on test vehicle-2 through exposure to 150°C for 60 days prior to the initiation of testing under combined temperature and vibration. Material properties of the printed circuit board at test temperature have been measured using tensile tests and dynamic mechanical analysis. The vibration simulation using global-local FE models is correlated with the system characteristics such as modal shapes and natural frequencies and displacement amplitudes for each temperature. Full field strain has been extracted using high speed cameras in conjunction with digital image correlation. Stresses in solder interconnects have been extracted from sub-model and stress amplitude is plotted against cycles to failure at all the test temperatures. This study presents a comparison of failure modes for various alloy compositions at elevated test temperature and vibration for different aging conditions. Anand Viscoplasticity material data from the prior studies by the authors have been used to capture the high-strain rate temperature dependent aging behavior of the solder joints. Finite element models have been used to predict the combined effect of temperature and vibration on the reliability of solder joints. Model predictions have been correlated with experimental data.

TEST VEHICLE

Two test vehicles were used in the study of simultaneous exposure to temperature and vibration. Test vehicles are representative of engine control unit of an agriculture equipment. Test Vehicle-1 has daisy chained PBGAs, QFP, TSOP and SOL packages with SAC305 lead free solder interconnects. Test vehicle-1 is a 4-layer, 1.56mm thick test board with immersion silver finish. Dimensions of Test vehicle 1 are 204mm x 129mm. Test Vehicle-2 has 12 identical daisy chained CABGA packages. Two configurations of the test vehicle-2 were fabricated. One with SAC105 parts and the second with SAC305 parts on the test board. Test Vehicle-2 is an 8-layer, 1.6mm thick test board with immersion silver finish. Test Vehicle-2 is 132mm in length, and 77mm in width. The PCB pads are non-solder mask defined (NSMD) for the both test vehicles. Test vehicle-1 and 2 are shown in Figure 1, and Figure 2. Package attributes for both the test vehicles are shown in Table 1. All the packages used for the study were subjected to x-ray inspection to measure the size of the embedded features in addition to the chip size.

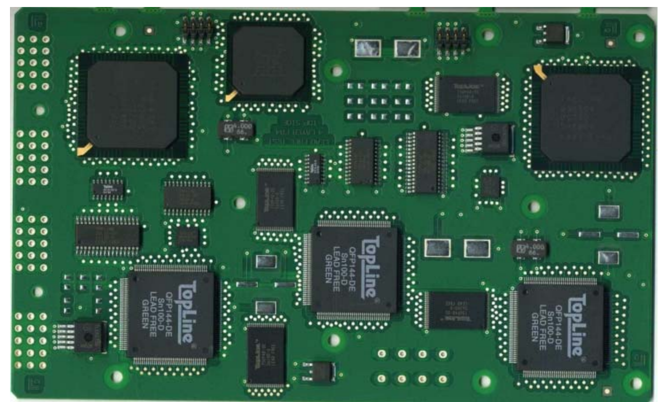

Figure 1: Test Vehicle 1

Figure 2: Test Vehicle 2

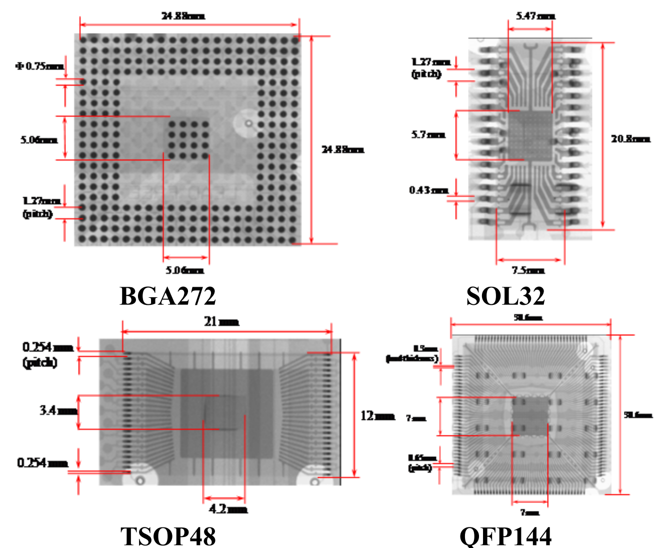

Figure 3: X-ray Images of Packages on Test Vehicle 1

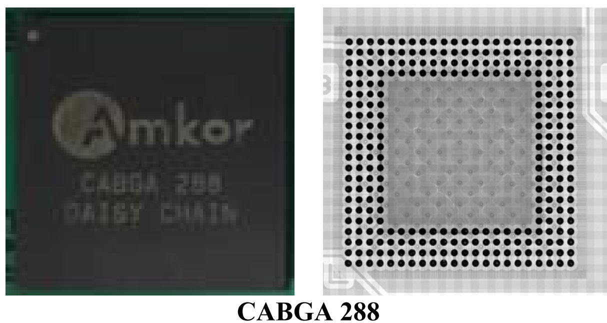

CABGA 288

Figure 4: X-ray Images of Packages on Test Vehicle 2.

Table 1: Package Attributes

Test Vehicle 1				
Package	Pitch (mm)	Ball Dia.	Solder Alloy	I/O Count
BGA	1.27	0.75	SAC305	272
QFP	0.65	0.33	SAC305	144
SOL	1.27	0.43	SAC305	32
TSOP	0.5	0.254	SAC305	48
Test Vehicle 2				
CABGA	0.8	0.46	SAC105 SAC305	288

Table 2: Test Conditions for Test Vehicle-1

Test Vehicle 1		
Test Temp.	Vibration Level	Solder Alloy
25	10g	SAC305
75	10g	SAC305
125	10g	SAC305

Table 3: Test Matrix for Test Vehicle-2

Test Temp (C)	***Test Vehicle 2*** Stress Level: 14 g			
	SAC105		SAC305	
	No aging	60 Days	No Aging	60 Days
25	X		X	
55		X		X

X-ray images for both the test vehicles are shown in Figure 3, and Figure 4. The attributes of all packages are on the test vehicles are shown in Table 1. Table 2, and Table 3 show the test conditions of vibration and temperature that have been used to test the board assemblies. Test Vehicle -1 is subjected to 10g and Test Vehicle-2 is subjected to 14g at elevated temperatures.

EXPERIMENTAL SETUP

A LDS Shaker V722 has been used for this study with an isothermal oven to simulate the simultaneous exposure to vibration at elevated temperatures. Isothermal oven is equipped with a glass window on top-surface to allow acquisition of transient dynamics using high speed imaging of PCB deformation. Test vehicle-1 and 2 have been subjected to sinusoidal vibration at their first natural frequency of the test board assembly with an acceleration amplitude of 10g and 14g while being exposed to elevated temperature. Resistance for all the packages under test has been monitored using a high-speed data-acquisition system. A resistance increase of 20-percent over the initial resistance for period of over 20-cycles or more compared to that of a pristine assembly has been deemed as a failure of the assembly. All the board assemblies in the test matrix have been tested till failure definition. The cycles to failure have been counted using the time to failure and the resonant frequency of the test assembly. Figure 5 shows the experimental setup along with shaker system, thermal chamber, high speed imaging, data acquisition system, and the shaker controller. The resistance of different daisy chained packages have been monitored using high speed data logger.

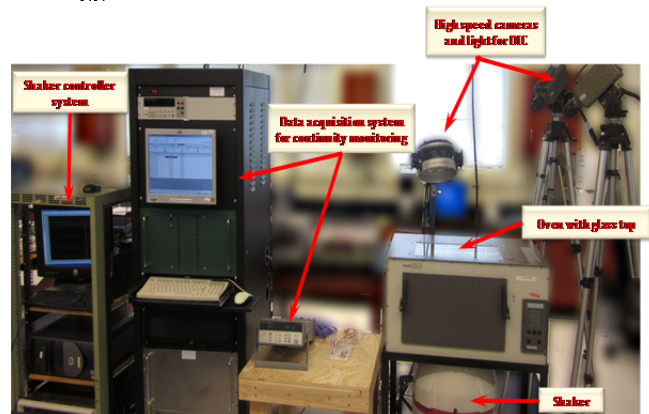

Figure 5: Experimental Setup

APPROACH TO LIFE-PREDICTION MODELING

Experimental model analysis has been used to identify the frequencies of the first few mode shapes. The board assemblies have been subjected to vibration at the first model frequency at several temperatures in the range of operational temperatures for automotive underhood applications. For the purpose of modeling, tensile tests, and dynamic mechanical analysis has been performed to measure the PCBs properties. Full field strain has been extracted using high speed cameras in conjunction with digital image correlation while the boards were subjected to high temperature vibration. Finite element predictions of the displacement field of the board assembly have been correlated with the measurements of the displacement field using DIC in conjunction with high speed imaging. Stresses in solder interconnects have been extracted from the validated sub-model and stress amplitude is plotted against cycles to failure at all the test temperatures. Anand Viscoplasticity material data from the prior studies by the authors have been used to capture the high-strain rate temperature-dependent aging behavior of the solder joints. Finite element models have been used to predict the combined effect of temperature and vibration on the reliability of solder joints. Figure 6 shows the approach to high cycle fatigue life prediction for solder alloys at elevated temperatures.

Figure 6: Flowchart to calculate S-N Curves at elevated temperatures.

MODAL ANALYSIS:
An experimental Modal Analysis (EMA) is conducted on both test vehicles to measure the 1st Natural frequency (1st NF) shown in Figure 7, Figure 8. The test vehicles were subjected to harmonic vibration at their 1st NF at elevated temperatures.

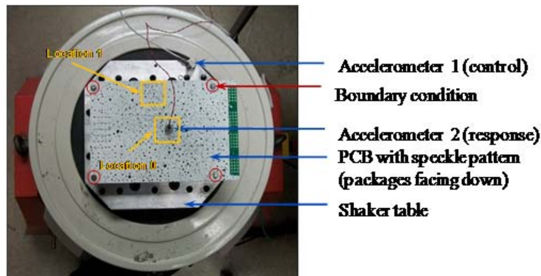

Figure 7: Board Configuration and Location of Accelerometers for Modal Analysis for Test Vehicle-1

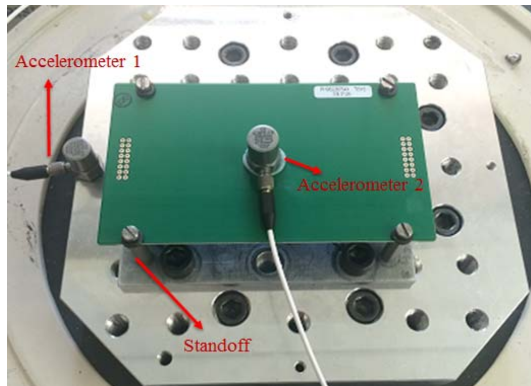

Figure 8: Board Configuration and Location of Accelerometers for Modal Analysis for Test Vehicle-2

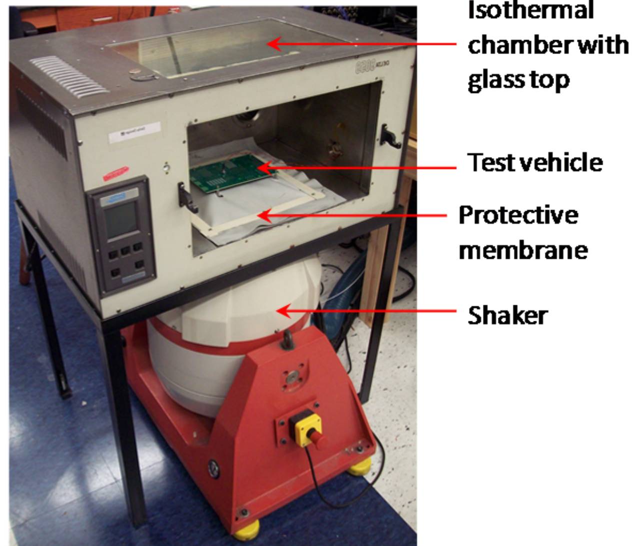

Figure 9: Board Configuration for High Temperature Vibration on Shaker inside a Thermal Chamber

Two accelerometers have been mounted, one on the shaker, and the second on the board in order to measure the receptance of the board assemblies as shown in Figure 8. One accelerometer is attached to shaker table and other one is attached at center of test board as shown in Figure 7, Figure 8. Accelerometer 1 measures the excitation signal and Accelerometer 2 measure the response. The test board with package facing down is mounted on four standoffs. A sine sweep profile from 5 Hz to 2000 Hz with constant amplitude of 10 G is used. A transmissibility plot is obtained from EMA test as shown in Figure 10. The excitation frequency corresponding to each peak in the transmissibility plot denotes the natural frequency of test board.

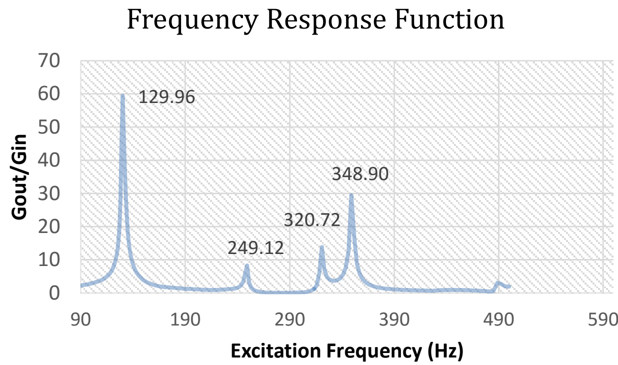

(a)

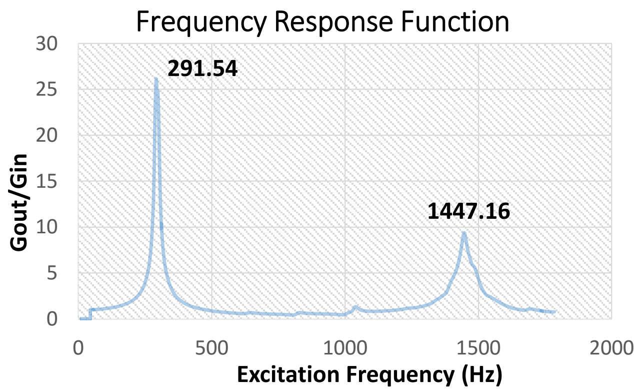

(b)

Figure 10: Frequency response plot (a) Test Vehicle-1 (b) Test Vehicle-2.

MEASUREMENT OF DAMPING RATIO

For a system excited close to its resonant frequency, the damping ratio becomes a very critical dynamic characteristic. It enforces steady state of the response of the system. Half-power bandwidth method shown in Eq. (1) is used for lightly damped structures.

$$\xi = \frac{\Delta f_n}{2 f_n} \tag{1}$$

where ξ is the damping coefficient, f_n is the natural frequency and Δf_n is the difference in half-power bandwidth frequencies. Figure 11 shows the acceleration response from 100Hz to 150Hz. f_n=129.96Hz and Δf_n=3.5Hz at 25°C for clarity. So the damping ratio is 0.013. The damping coefficient can further be split into Raleigh coefficients - mass damping coefficient and stiffness damping coefficient.

$$\alpha = \xi \frac{2 \times \omega_1 \times \omega_2}{\omega_1 + \omega_2} \tag{2}$$

where α is the mass damping coefficient. Substituting for the terms on the RHS of Eq. (2)

$$\alpha = 0.013 \frac{2 \times 2\Pi \times (132 \times 128.5)}{132 + 128.5} \tag{3}$$

$$\alpha = 10.64 \tag{4}$$

The stiffness damping coefficient is given by:

$$\beta = \xi \frac{2}{\omega_1 + \omega_2} \tag{5}$$

$$\beta = 0.013 \frac{2}{2\Pi(132 + 128.5)} \tag{6}$$

$$\beta = 1.59 \times 10^{-6} \tag{7}$$

It can be seen by comparing Eq.(4) and Eq.(7) that the mass damping is higher than the stiffness damping for this structure.

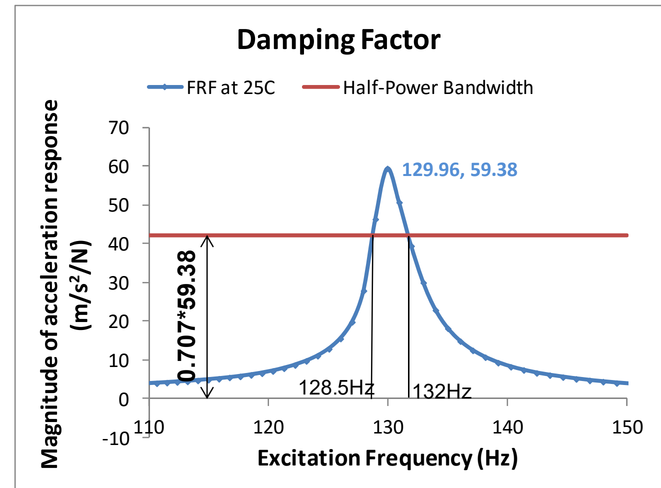

Figure 11: Half power bandwidth method for damping coefficient

DEVELOPMENT OF THE GLOBAL FE-MODEL

The global model built for FE simulations is shown in Figure 12 for test vehicle-1 and in Figure 13 for test vehicle-2. The models for the two test assemblies have been developed using different strategies. The test vehicle-1 has been developed using smeared material properties for a number of element layers. The global model for test vehicle-1 has been used in conjunction with a local model described later in the paper.

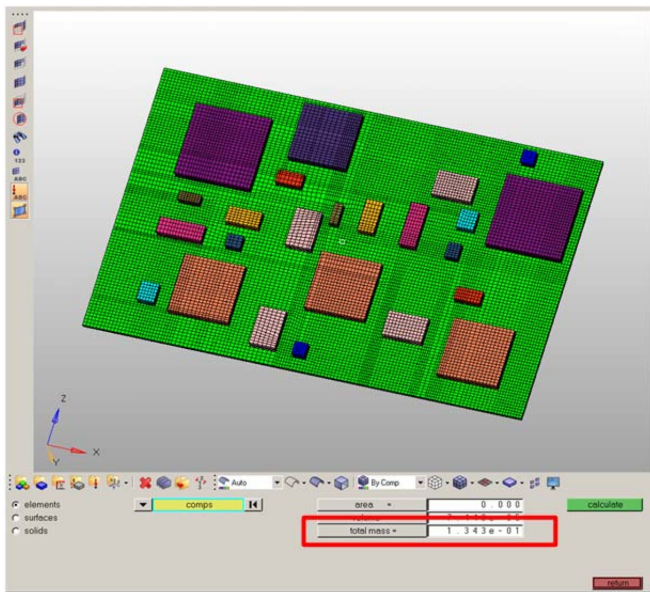
Figure 12: Global model for modal dynamic analysis to simulate board deflection for Test Vehicle-1

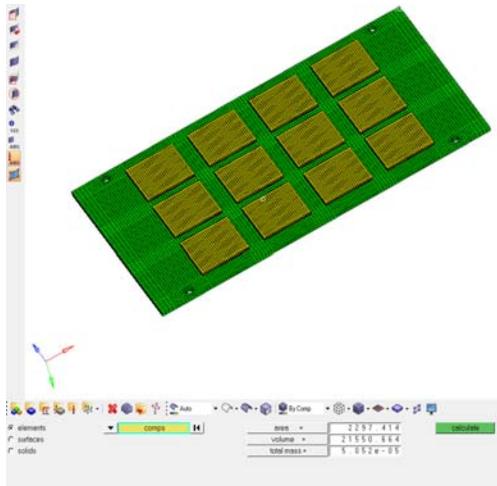
Figure 13: Global model for modal dynamic analysis to simulate board deflection for Test Vehicle-2

The primary purpose of the global model is to predict the natural frequencies, and global displacements under a vibration load. However, since the solder layer has been smeared in test vehicle-1, local sub-models have been developed for each of the components on test vehicle-1. The sub-models capture the dimensions details of the solder joints and the embedded layers inside the semiconductor package.

The model for test vehicle-2 has been developed using Timoshenko beam elements with actual embedded layer dimensions. Since, the global model has interconnects included as Timoshenko-beam elements, no sub-models are needed for the test vehicle-2.

Test Vehicle-1

Smeared properties are used for the components on the global model of Test-Vehicle-1. In this approach, the component is modeled as block like structure omitting the geometric and material details (Figure 14).

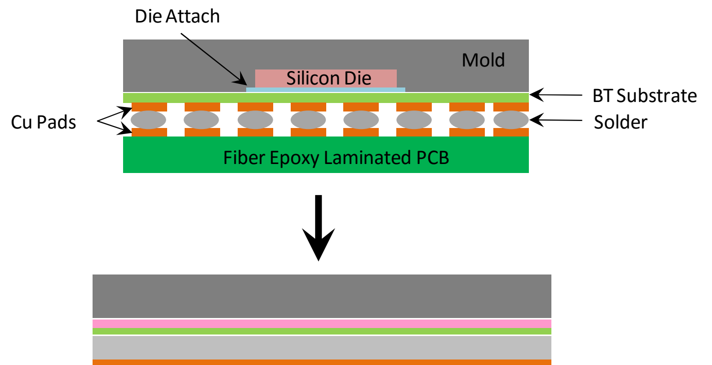

Figure 14: Smeared property model

The component is then assigned equivalent material properties based on the multi-layer structure of the component. Eq.(8) gives the effective Poisson's ration based on the rule of mixtures widely applied in composite materials [Clech 1997]. The effective Young's Modulus is obtained by Eq. (9) using the additive property of the bending property of individual layers of the component. The equivalent density in Eq. (10) is the volumetric average of the densities of the layers.

Table 4 lists the calculated properties for the components. The temperature effect on the solder property deterioration has a noticeable impact on the effective Young's Modulus of PBGAs.

$$\upsilon_{eff} = \sum_i^n \upsilon_i h_i \Big/ \sum_i^n h_i \quad (8)$$

ν_{eff} is the effective Poisson's ration of the component ν_i and h_i are the Poisson's ratios and heights of the layers of the multi-layer stack.

$$\frac{E_{eff} h_{eff}^3}{12(1-\upsilon_{eff})} = \sum_i^n \frac{E_i h_i^3}{12(1-\upsilon_i)} \frac{\Delta f_n}{2 f_n} \quad (9)$$

E_{eff} and h_{eff} are the effective Elastic Modulus and height of the component E_i is the Elastic Modulus of each i layers of the multi-layer stack.

$$\rho_{eff} = \sum_i^n \rho_i V_i \Big/ \sum_i^n V_i \quad (10)$$

ρ_{eff} and is the effective density and V_i is the volume of each of the i layers of the multi-layer stack. The global model was followed with a local model for each of the semiconductor packages in the electronic assembly. Tensile test is used to measure mechanical properties such as Elastic modulus. PCB and other components is modeled using material properties shown in

Table 4 for Test Vehicle-1.

Table 4: Smeared Properties used for Test Vehicle-1

Component	Density (kg/m^3)	Poisson Ratio	E (GPa)
PCB		0.33	23.80
BGA272	2118.5	0.27	4.962
BGA388	1987.3	0.39	4.366
QFP144	1976.4	0.25	12.70
TSOP	1962.1	0.27	8.294
SOL	1997.7	0.26	9.300

Test Vehicle-2

For Test Vehicle-2, the smearing scheme was not used for the analysis of test vehicle-2. Test vehicle-2 is modeled using material properties detailed in Table 5.

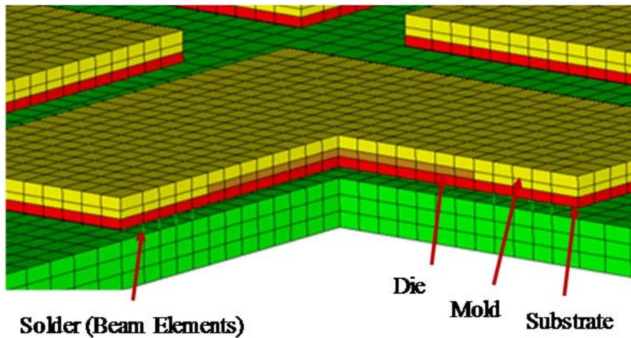

Figure 15: Global FE Model of Test Vehicle-2 with Timoshenko Beam Elements.

For solder interconnects, Timoshenko beam elements (BEAM188) is used. Tensile test is used to measure mechanical properties such as Elastic modulus. PCB and other components is modeled using material properties shown in Table 5 for Test board 2.

Table 5: Material Properties used for Test Vehicle-2

Component	Density tonne/mm^3	v	E (GPa)	Element Type
PCB	1.80E-09	0.39 0.17	20.8 24.8	SOLID45
Mold Compound	1.65E-09	0.25	23.5	SOLID45
Silicon Die	1.65E-09	0.28	162	SOLID45
BT Substrate	1.65E-09	0.28	17.4	SOLID45
SAC105 SAC305	1.65E-09	0.34	43 42	BEAM188

Validation Check for the Final Model Weight

The mass of the model for test vehicle-1 is 134.3 gram and the model for test vehicle-2 is 50.52 gram using smeared properties for the packages (Figure 16). The model weight has been compared with the measured weight of the board assembly. Table 6 shows that model weight correlates well with the actual weight of the board assembly.

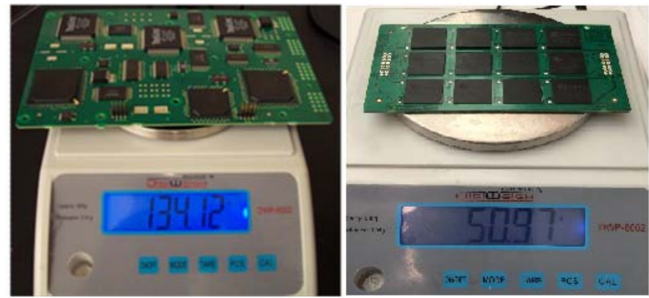

Figure 16: Weight of Experimental Test Board

Table 6: Comparison of Actual weight and FE based Global Model Weight

Test Vehicle	Actual (gm)	FE Model (gm)
Test Board 1	134.12	134.3
Test Board 2	50.97	50.52

MODEL PREDICTIONS OF NATURAL FREQUENCIES AND MODE SHAPES

The model predictions of the natural frequencies have been compared with the experimental measurements for both test vehicle-1 and test vehicle-2. Furthermore, digital Image correlation has been used in conjunction with high speed imaging to correlate the mode shape and the full field displacements of the FE model. Digital image correlation (DIC) is an optical method to measure full-field deformation and the derivatives of deformation on the surface of a structure. Previously, the feasibility of using DIC for transient strain measurement in electronic assemblies, in the presence of rigid body motion has been demonstrated [Lall 2007a-e, 2008a-d]. The technique involves the application of speckle pattern on the surface of the printed circuit board assembly and tracking geometric points on the speckle patterned surface before and after loading and using them to compute both in-plane as well as out-of-plane deformations in the structures. [Zhou 2001,Amodio 2003, Srinivasan 2005, Kehoe 2006, Lall 2007c, 2008c,d]. Figure 17 shows the principle of DIC in a three-dimensional case. The sub image before deformation is referred as I1 (r) and the one after impact is referred as I2 (r) respectively.

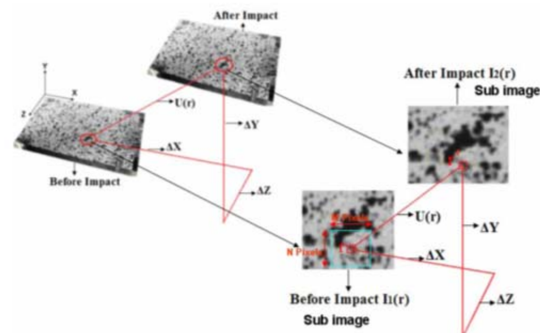

Figure 17: 3D-Digital Image Correlation measurements in Printed Circuit Assembly

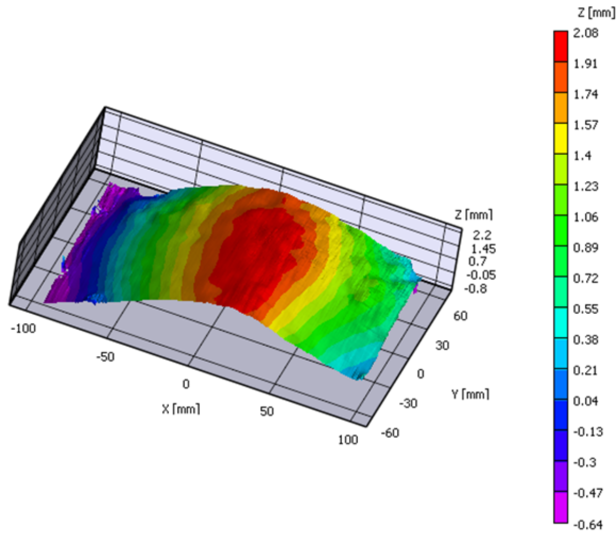

(a)

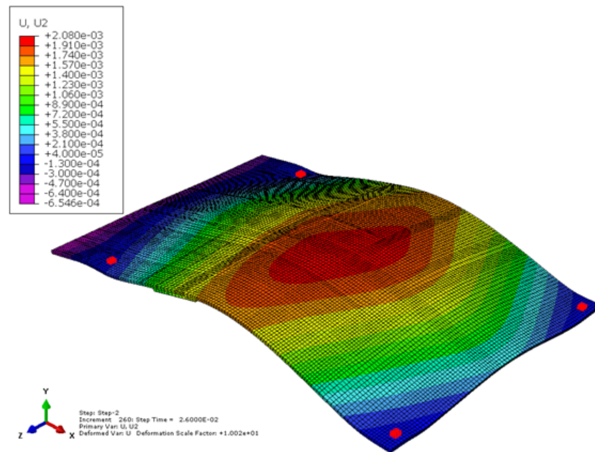

(b)

Figure 18: (a) Test Vehicle-1 experimental mode shape at 1st NF (b) Test Vehicle-1 FE mode shape at 1st NF.

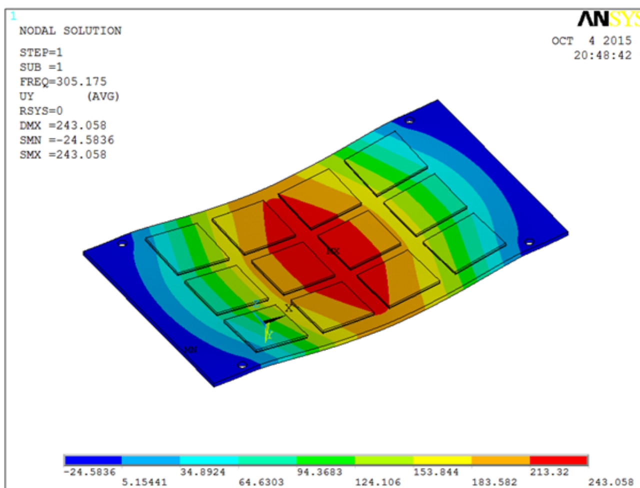

Figure 19: 1st Mode Shape and full field out of plane displacement contour at 1st NF of Test Vehicle 2 from FE.

Figure 18 shows a comparison of mode-1 deformation mode shape from DIC and the finite element model, both conducted at 25°C, 10g and first natural frequency. Model predictions of the mode-shape correlate well with the experimental measurements. Figure 19 shows the model prediction of mode shape for the first natural frequency for test vehicle-2. Furthermore, the model predictions of the first three natural frequencies has been compared with the experimental measurements. Table 7 shows comparison of natural frequencies obtained from EMA and FE modal analysis. Model predictions of the natural frequencies correlate well with the experimental measurements for both test vehicle-1 and test vehicle-2. From the comparison of natural frequencies, and mode shape out of plane displacements and in-plane strains, the global model can be said to correlate well with experimental measurements for both the test vehicles.

Table 7: Natural Frequency

Test Vehicle 1			
Mode	Natural Frequency (Hz)		Error (%)
	Experimental	FE Simulation	
Mode 1	129.9	129.1	0.59
Mode 2	249.1	247.5	0.60
Mode 3	320.9	305.7	4.68
Test Vehicle 2			
Mode 1	290.7	305	-4.91
Mode 2	693.8	670.8	3.31
Mode 3	896.5	794.7	11.3

MODEL PREDICTIONS OF OUT-OF-PLANE DISPLACEMENTS

Displacement field ranges from -0.06mm to 2mm in DIC and -0.065mm to 2mm in modal dynamic analysis. PCB out of plane displacement and in-plane strain along the length captured by DIC correlate well with those predicted by FEA at the same point A(50,60) at all the test temperatures (Figure 20). FE model predictions for displacement and strain are slightly lower in amplitude than the experimentally measured DIC values in all the cases but correlate well with the experimental measurements in all the cases.

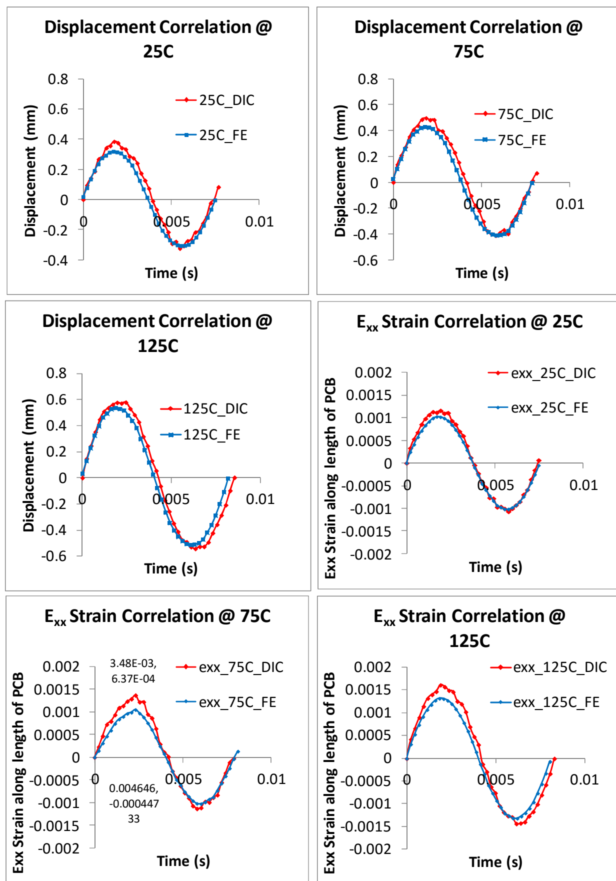

Figure 20: Correlation of PCB Out of plane displacement and in-plane strain

LIFE DISTRIBUTIONS

Test vehicle-1 has multiple component architectures with SAC305 while test vehicle-2 has identical components at a number of different locations on the test board in two configurations including SAC105 and SAC305. Since the focus of the study is on the development of life prediction models for solder joint reliability under simultaneous exposure to temperature and vibration, only life-data which involves solder joint failure has been used for the purpose of development of the damage relationship. The failure has been defined as the increase of 20-percent in (ΔR/R) for consecutive 20-cycles or a resistive open which ever one happens first. Cycles to failure differ for every package because each component location experiences different strain levels based on its location on the test board. The cycles to failure have been calculated by multiplying the time to failure by frequency of base excitation which is constant throughout the test. Typical resistance vs time plots are shown in Figure 21 for test vehicle-1. Further, Figure 22 shows the resistance versus time data for the SAC105 configuration of test vehicle-2. Furthermore, the resistance versus time data for the SAC305 configuration of test vehicle-2 is shown in Figure 23. Cycles to failure for each package as a function of test temperature are plotted in Figure 24. There is a difference in mean cycles to failure as the temperature is increased from 25°C to 125°C. Since the test vehicles were assigned randomly to a test case, the difference in mean cycles to failure can be attributed to test temperature.

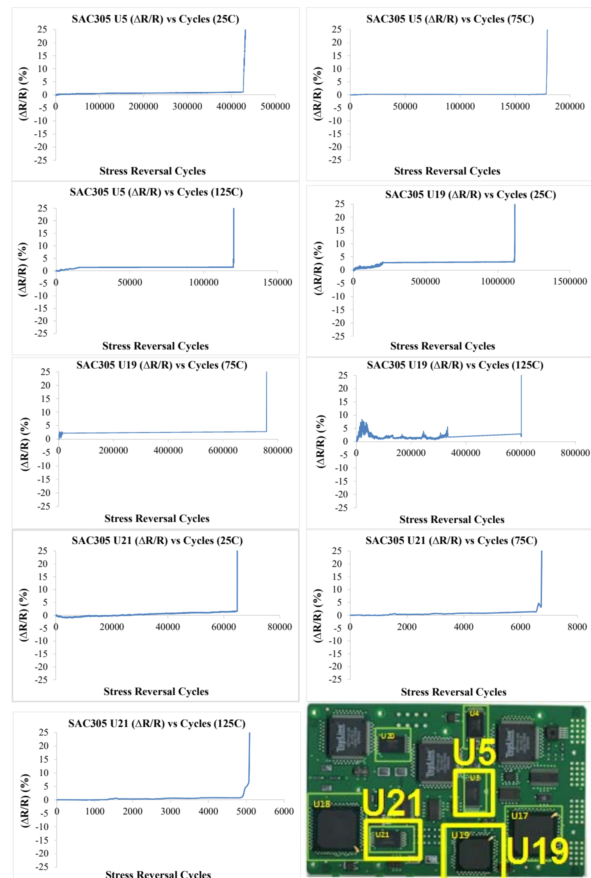

Figure 21: Resistance vs cycles to failure for test vehicle-1

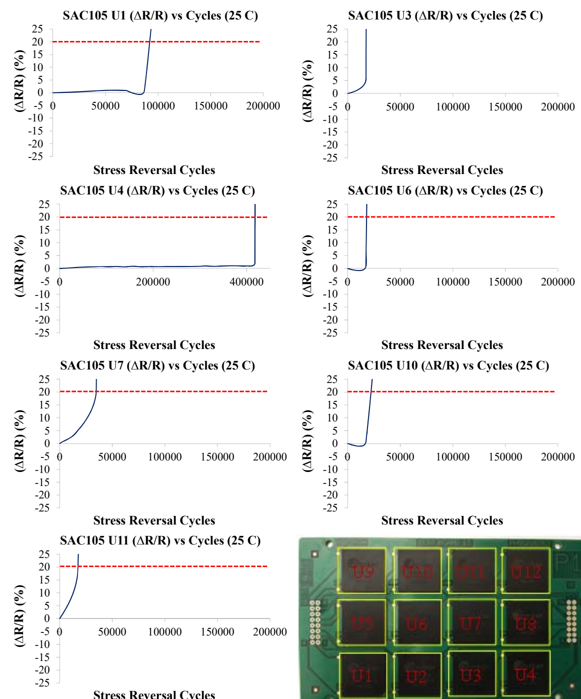

Figure 22: Resistance vs cycles to failure for SAC105 configuration of test vehicle-2

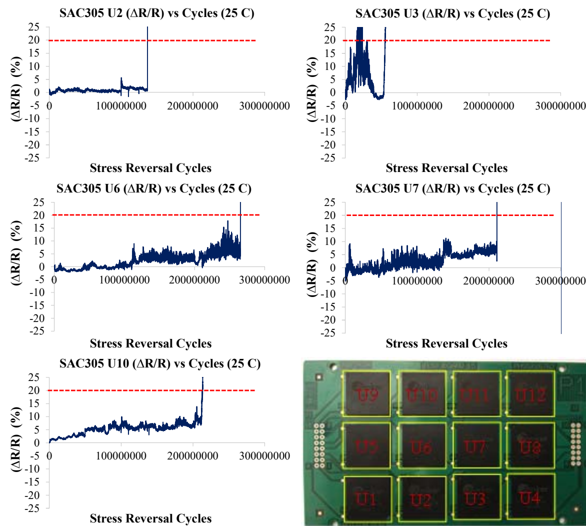

Figure 23: Resistance vs cycles to failure for SAC305 configuration of test vehicle-2

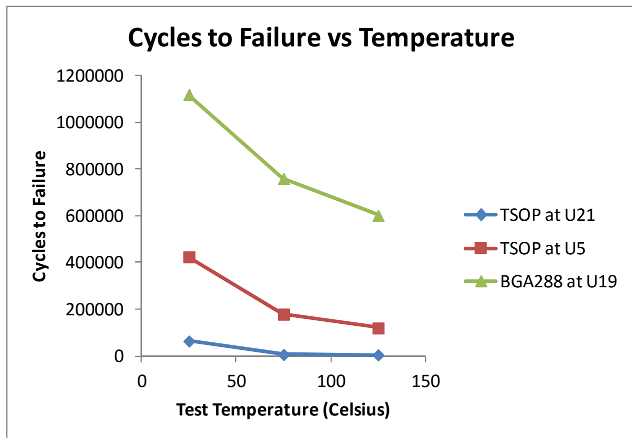

Figure 24: Difference in means of cycles to failure due to change in test temperature for SAC305 solder joints.

SOLDER STRESS ESTIMATION FROM EXPLICIT SUBMODELS

Explicit finite element models have been developed to model the vibration of the test boards. Model predictions have been used to determine the interconnect strain histories. Reduced integration elements have been used for computational efficiency, since the internal load vector scales with the number of integration points. Computational time of the dynamic event is reduced by incorporating reduced integration elements in the analysis because these element types use fewer integration points to form the element stiffness matrices. Lower order elements have been implemented since they perform better when the strain is large or very high strain gradient is expected during vibration cycle. Three-dimensional continuum elements C3D8R have been used to model the components layers of printed circuit board, substrate, mold, leads, lead-frame, solder, corner solder balls, die, die paddle and copper pad. In PBGAs, except the four corner interconnects, all remaining interconnects have been modeled as Timoshenko beam elements (Figure 25). Displacement boundary conditions of the sub-models are derived from the global model. Explicit dynamic analysis is conducted to obtain solder stresses. High strain rate solder material properties at the three test temperatures are tabulated in Table 8. The degradation in material properties is assumed to be in-line with other SAC alloys.

Table 8: SAC305 Solder material properties [Lall 2012]

Temperature (Celsius)	Elastic Modulus (GPa)	UTS (MPa)
25C	40	100
75C	30	90
125C	20	80

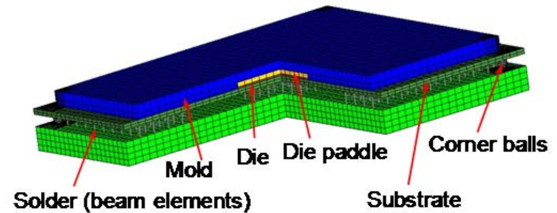

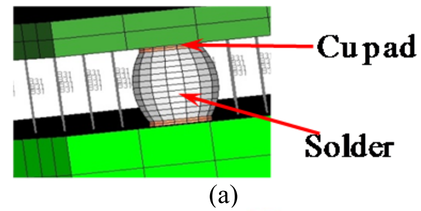

(a)

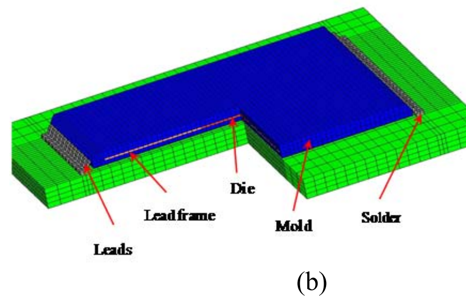

(b)

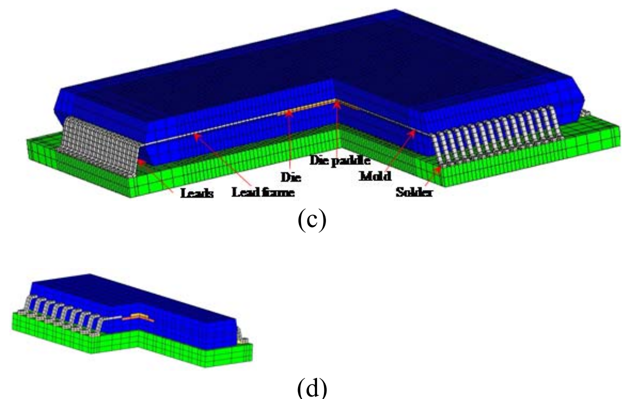

(c)

(d)

Figure 25: (a) BGA (b) TSOP (c) QFP (d) SOL sub-models

The solder interconnects experience tension-compression as well as shear stress in a vibration test. For fatigue life prediction, an equivalent stress of the solder interconnects needs to be considered. Therefore an equivalent stress called Von Mises stress is used for constructing the S-N curve.

shows the stress contour in solder balls of BGA and TSOP. Volumetric average stress value is used in the region of solder/PCB interface so that mesh density does not have a significant effect on stress distribution. Eq. (14) is used to derive volume averaged stress.

$$\sigma_{avg} = \frac{\Sigma\sigma \times V}{\Sigma V} \tag{11}$$

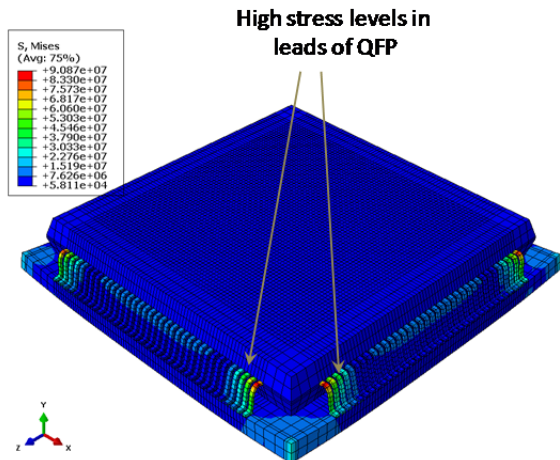

Figure 26: QFP high stresses in corner and mid-side leads

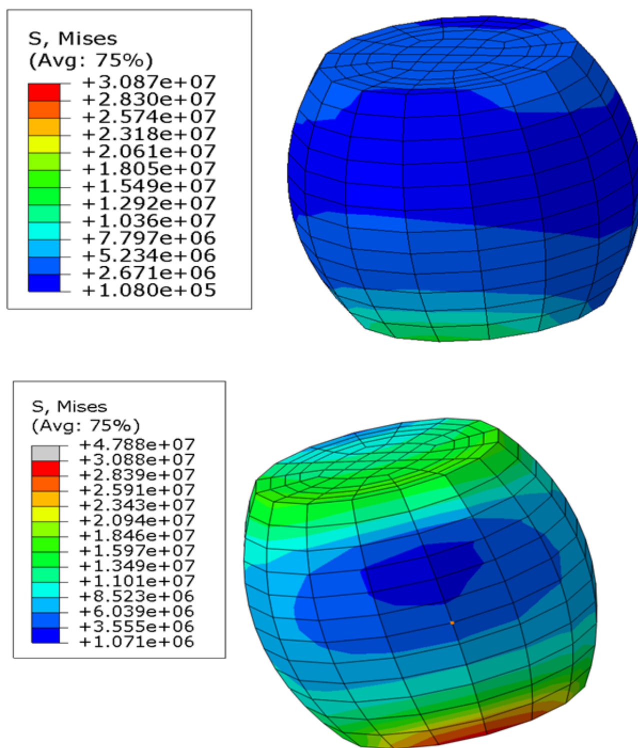

Figure 27: (a) U19 Corner solder ball Mises stress distribution at 125C (b)U19 corner solder stress distribution at 25°C

Solder stress levels for BGA and TSOP reduce with increase in temperature. High stresses are observed in corner solder ball at the PCB side. Similarly, high stresses are observed in corner leads and solder underneath these leads in TSOPs. The failure mode in BGA and TSOP obtained during tests is captured well in the simulation. [Figure 27, Figure 28]. The stress histories are denoted in Figure 29

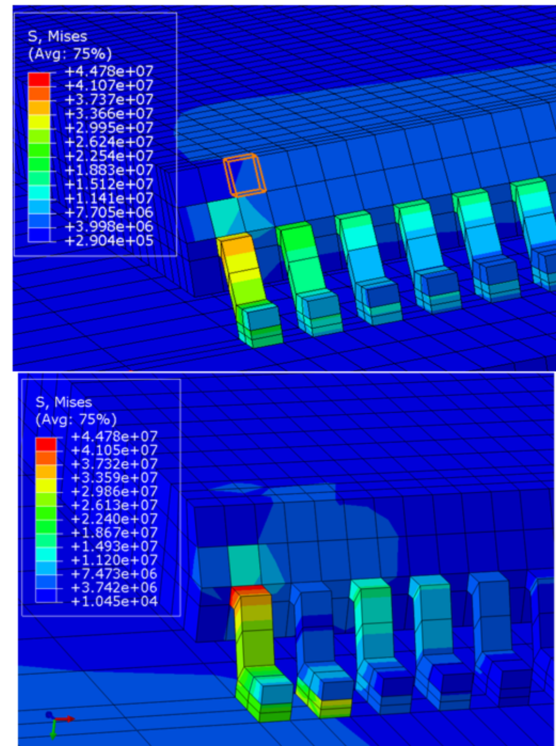

Figure 28: (a)U5 Corner solder Von Mises stress distribution 125C (b)U5 corner stress distribution at 25C

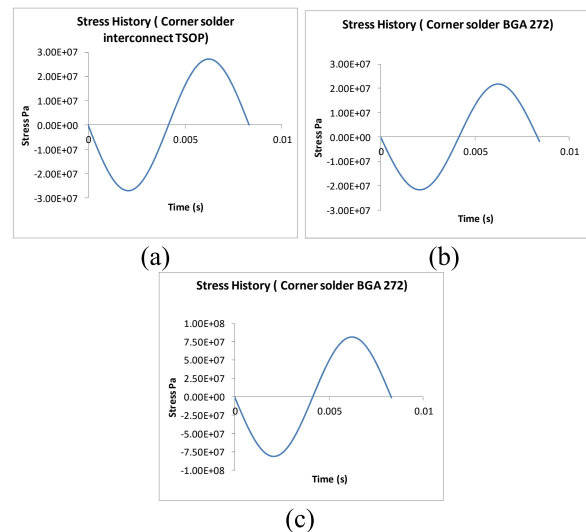

Figure 29: Stress histories at 125C from a) TSOP submodel corner solder b) BGA submodel corner solder c)QFP corner lead

High cycle fatigue failure is characterized by Basquin power law relation:

$$\sigma_a = \sigma_f (2N_f)^b \tag{12}$$

Table 9 lists the fatigue coefficients published in literature for various solder alloys. S-N curve obtained in this study is plotted on a log-log scale as shown in Figure 30. The procedure is repeated for all test temperatures to obtain two additional S-N curves. While the cycles to failure reduce with increase in temperature, the failure threshold also decreases with increase in temperature due to degradation of material properties (Figure 30).

Table 9: Published values of Solder Fatigue Constants

Author	Alloy	σ_f (MPa)	b	R^2
Yu 2011	SAC305	64.8	-0.1443	0.77
Yu 2011	SAC405	152.2	-0.2079	0.97
Mason 1964	63Sn37Pb	66.3	-0.12	
Yao 1999	63Sn37Pb	177.15	-0.2427	
Steinberg 2001	63Sn37Pb	109.6	-0.1	
CAVE3	SAC305	65.193	-0.071	0.997

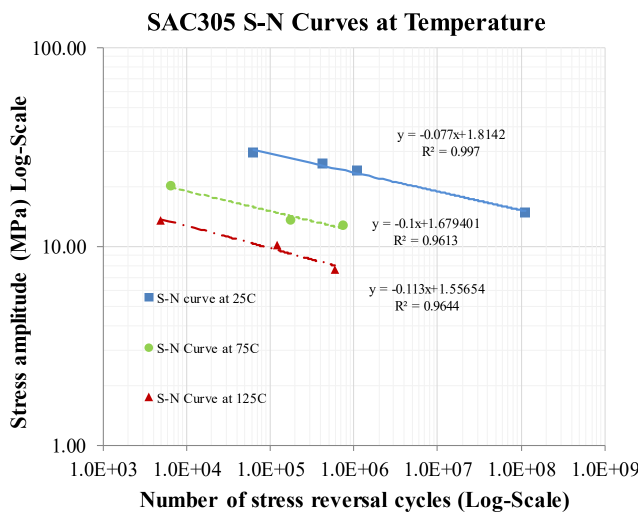

Figure 30: SAC305 Curve fitting at 25C

The coefficients σ_f and b evolve with temperature as shown in the table below. The reduction in σ_f and b causes a shift in the S-N curves with increase in temperature as shown in Figure 30. This change can be attributed to the evolution of microstructure of SAC305. Figure 31 shows the evolution of phase structure as seen in SEM within just one day of aging at 75C and 125C [Lall 2004a-d, 2005a-b, 2006a-f, 2007a-e, 2008a-f, 2009a-d, 2010a-j, 2011, 2012].

Table 10: SAC305 Fatigue strength coefficient and exponent at temperature

Temperature (Celsius)	σ_f (MPa)	b
25	70.08	-0.077
75	47.797	-0.1
125	36.02	-0.113

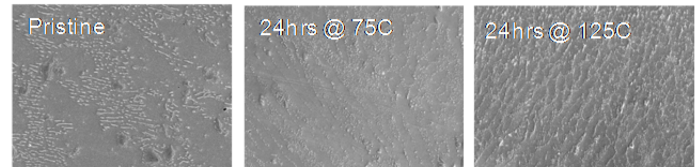

Figure 31: SAC305 phase growth [Lall, 2012]

The fatigue coefficient and the fatigue exponent decrease with increase in temperature. Based on Arrhenius theory, the relation between the fatigue strength coefficient and temperature is assumed to be of the form given by Eq. (13)

$$\sigma_{f,T} = \sigma_{f,0} \times e^{E_{A,\sigma_f}/KT} \tag{13}$$

where $\sigma_{f,T}$ is the fatigue strength coefficient at temperature T Kelvin, K is the Boltzmann's constant and Ea, σ_f is the activation energy in eV.

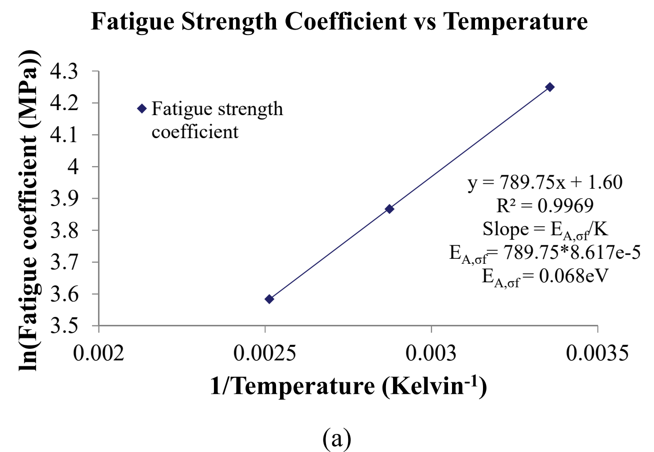

(a)

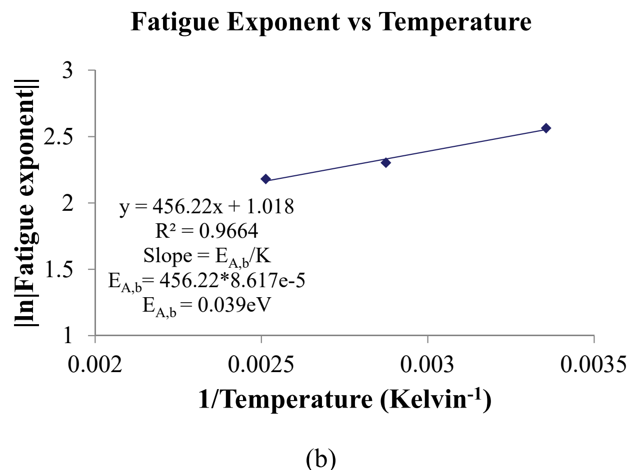

(b)

Figure 32: (a) SAC305 Fatigue coefficient as a function of temperature (b) SAC305 Fatigue exponent as a function of temperature

Taking natural log of both sides of Eq. (13) and then substituting the slope and intercept values from Figure 32a:

$$\ln \sigma_{f,T} = \ln \sigma_{f,0} + \frac{E_{A,\sigma_f}}{KT} \tag{14}$$

$$\ln\sigma_{f,T} = 1.6 + \frac{789.75}{T} \tag{15}$$

Taking antilog:

$$\sigma_{f,T} = 1.6 \times e^{789.75/T} \tag{16}$$

Similarly, considering the magnitude of fatigue coefficient b as a function of absolute temperature:

$$b_T = b_0 \times e^{E_{A,b}/KT} \tag{17}$$

Taking natural logarithm of both the sides,

$$\ln b_T = \ln b_0 + \frac{E_{A,b}}{KT} \tag{18}$$

Substituting slope and intercept from Figure 32b:

$$\ln b_T = -\left[1.018 + \frac{456.22}{T}\right] \tag{19}$$

Taking into account the negative sign of the exponent,

$$b_T = -\left[1.018 \times e^{-456.22/T}\right] \tag{20}$$

Activation energy for the fatigue coefficient is 0.06eV. The activation energy for Sn-Pb solder creep found in literature is about 0.5eV for grain boundary creep and 0.84 eV for matrix creep [Knecht 1990]. To account for the effect of temperature in predicting the fatigue life of SAC305, Eq.(16) and Eq. (20) that give the temperature dependence of these parameters can be substituted in the Basquin power law relation given by Eq.(12)

$$\sigma_a = \left[\sigma_{f,T}\right] \cdot (2N_f)^{b_T} \tag{21}$$

Thus the high cycle fatigue life of SAC305 as a function of temperature can be expressed in terms of Basquin power relation as follows:

$$\sigma_a = \left[1.6 \times e^{\frac{789.75}{T}}\right] \cdot (2N_f)^{-\left[1.018 \times e^{-456.22/T}\right]} \tag{22}$$

where σ_a is the stress amplitude in MPa, T is the test temperature in Kelvin and $2N_f$ is cycles to failure.

SUMMARY AND CONCLUSIONS

Solder joint reliability for SAC105 and SAC305 alloys has been studied in two test vehicles under simultaneous temperature and vibration. Board assemblies have been subjected to two acceleration levels of 10g and 14g over temperature range of 25°C to 125°C. Resistance of the components has been measured during the test till failure. The board assemblies have been modeled using finite elements to extract the stress amplitude in the solder joints during exposure to simultaneous temperature-and-vibration. Volume averaged solder stresses at high stress location of every component is plotted against its experimentally obtained cycles to failure. S-N curves for SAC305 are obtained based on Basquin power law relation between stress amplitude and stress reversal cycles. S-N curves at 25C, 75C and 125C are thus obtained for SAC305. A temperature dependent form of the Basquin power law has been presented for the SAC305 solder under simultaneous temperature-vibration. The temperature dependence of the fatigue strength coefficient and fatigue exponent has been computed from the SAC305 S-N curve relation using Arrhenius relationship. The temperature dependent forms of the fatigue coefficient and fatigue exponent have been implemented in Basquin power relation. The temperature dependent form of the Basquin Power Law can be used for the life prediction of the SAC305 solder joint reliability under exposure to temperature and vibration.

ACKNOWLEDGEMENTS

The research presented in this paper has been supported by NSF Center for Advanced Vehicle and Extreme Environment Electronics (CAVE^3) consortium-members.

REFERENCES

Al-Yafawi, A., Patil, S., Yu, D., Park, S., Pitarresi, J., and Goo, N., Random Vibration Test for Electronic Assemblies Fatigue Life Estimation, Thermal and Thermomechanical Phenomenon in Electronic Systems ITherm, pp. 1-7, June 2010.

Amodio, D., Broggiato, G., Campana, F., Newaz, G., Digital Speckle Correlation for Strain Measurement by Image Analysis, Experimental Mechanics, Vol. 43, No. 4, pp. 396- 402, 2003.

Barker, D., Vodzak, J., Dasgupta A., Pecht, M., Combined vibrational and thermal solder joint fatigue: A generalized strain versus life approach, Transactions ASME Journal of Electron. Packaging, Vol. 112, pp. 129–134, June 1990.

Barker, D., Vodzak, J., Dasgupta A., Pecht, M., PWB solder joint life calculations under thermal and vibrational loading, Journal of Institute of Environmental Science, Volume 35, No. 1, pp. 17–25, Feb. 1992.

Basaran, C., Chandaroy, R., Thermomechanical analysis of solder joints under thermal and vibrational loading, Transactions of ASME, Volume 124, pp. 60–66, Mar. 2002.

Clech J., Solder Reliability Solutions: A PC-Based Design-for-Reliability Tool, Proceedings of Surface Mount International, pp. 136-151, San Jose, CA, Sept. 8-12, 1996

Darveaux R., Reichman C., Islam N., Interface Failure in Lead Free Solder Joints, Proceedings of 56th ECTC, pp. 152-156, 2006.

Dehbi, A., Ousten, Y., Danto, Y., Wondrak, W., Microelectronics Reliability, Vol.45, pp. 1658-1661, 2005.

Gu, J., Cooreman, S., et al., Full-Field Optical Measurement for Material Parameter Identification With Inverse Methods, WIT Transactions on The Built Environment, Vol. 85, 2006.

Henderson, G., Piersol, A., Fatigue Damage Related Descriptor for Random Vibration Test Environments,

Sound and Vibration, Volume 29, No. 10, pp. 20–24, Oct. 1995.

Hu, J., Life Prediction and Damage Acceleration Based on the Power Spectral Density of Random Vibration, Journal of IES, Volume 38, No. 1, pp. 34–40. Jan/Feb. 1995.

Johnson, R., Evans, J., Jacobsen, P., Thompson, J., Christopher, M., The Changing Automotive Environment: High-Temperature Electronics, IEEE Transactions on Electronics Packaging Manufacturing, Vol.27, NO. 3, July 2004.

Kehoe, L., Lynch, P., Guénebaut, V., Measurement of Deformation and Strain in First Level C4 Interconnect and Stacked Die using Optical Digital Image Correlation, Proceedings of the 56th ECTC, pp. 1874-1881, May 2006.

Knecht, S., Fox, L., Constitutive Relation and Creep-Fatigue Life Model for Eutectic Tin-Lead, IEEE Transactions on Components, Hybrids and Manufacturing Technology, Vol. 13, No.2, June 1990.

Lall, P., Panchagade, D., Liu, Y., Johnson, W., Suhling, J., Models for Reliability Prediction of Fine-Pitch BGAs and CSPs in Shock and Drop-Impact, Proceedings of the 54th ECTC, pp. 1296-1303, 2004.

Lall, P., Panchagade, D., Choudhary, P., Suhling, J., Gupte, S., Failure Envelope Approach to Modeling Shock and Vibration Survivability of Electronic and MEMS Packaging, Proceedings of the 55th ECTC, pp. 480-490, 2005.

Lall, P., Gupte, S., Choudhary, P., Suhling, J. Solder-Joint Reliability in Electronics Under Shock and Vibration using Explicit Finite Element Sub-modeling, IEEE Transactions on Electronic Packaging Manufacturing, Volume 30, no. 1, pp. 74-83, January 2007a.

Lall, P., Choudhary, P., Gupte, S., Suhling, J., Hofmeister, J., Statistical Pattern Recognition and Built-In Reliability Test for Feature Extraction and Health Monitoring of Electronics under Shock Loads, 57th Electronics Components and Technology Conference, Reno, Nevada, pp. 1161-1178, May 30-June 1, 2007b.

Lall, P., Panchagade, D., Iyengar, D., Shantaram, S., Suhling, J., Schrier, H., High Speed Digital Image Correlation for Transient-Shock Reliability of Electronics, Proceedings of the 57th ECTC, Reno, Nevada, pp. 924-939, May 29 – June 1, 2007c.

Lall, P. Panchagade, D., Liu, Y., Johnson, W., Suhling, J., Smeared Property Models for Shock-Impact Reliability of Area-Array Packages, ASME Journal of Electronic Packaging, Volume 129, pp. 373-381, December 2007d.

Lall, P., Hande, M., Bhat, C., Islam, N., Suhling, J., Lee, J., Feature Extraction and Damage-Precursors for Prognostication of Lead-Free Electronics, Microelectronics
Reliability, Volume 47, pp. 1907–1920, December 2007e.

Lall, P., Choudhary, P., Gupte, S., Suhling, J., Health Monitoring for Damage Initiation and Progression during Mechanical Shock in Electronic Assemblies, IEEE Transactions on Components and Packaging Technologies, Vol. 31, No. 1, pp. 173-183, March 2008a.

Lall, P., Panchagade, D., Choudhary, P., Gupte, S., Suhling, J., Failure-Envelope Approach to Modeling Shock and Vibration Survivability of Electronic and MEMS Packaging, IEEE Transactions on Components and Packaging Technologies, Vol. 31, No. 1, pp. 104-113, March 2008b.

Lall, P., Iyengar, D., Shantaram, S., S., Gupta, P., Panchagade, D., Suhling, J., KEYNOTE PRESENTATION: Feature Extraction and Health Monitoring using Image Correlation for Survivability of Leadfree Packaging under Shock and Vibration, Proceedings of the 9th International Conference on Thermal, Mechanical, and Multi-Physics Simulation and Experiments in Micro-Electronics and Micro-Systems (EuroSIME), Freiburg, Germany, pp. 594-608, April 16-18, 2008c.

Lall, P., Iyengar, D., Shantaram, S., Pandher, R., Panchagade, D., Suhling, J., Design Envelopes and Optical Feature Extraction Techniques for Survivability of SnAg Leadfree Packaging Architectures under Shock and Vibration, Proceedings of the 58th Electronic Components and Technology Conference (ECTC), Orlando, Florida, pp. 036- 1047, May 27-30, 2008d.

Lall, P., Shantaran, S., Angral, A., Kulkarni, M., Explicit Submodeling and Digital Image Correlation Based Life-Prediction of Leadfree Electronics under Shock-Impact, 59th ECTC, San Diego, CA, pp. 542-555, May 25-29, 2009.

Lall, P., Limaye, G., Suhling, J., Murtuza, M., Palmer, B., Cooper, W., Reliability of lead-free SAC electronics under simultaneous exposure to high temperature and vibration, , 13th IEEE Intersociety Conference on Thermal and Thermomechanical Phenomena in Electronic Systems ITherm, pp. 753-761, May 2012.

Lall, P., Harsha, M., Suhling, J., & Goebel, K. (2012, May). Sustained damage and remaining useful life assessment in leadfree electronics subjected to sequential multiple thermal environments. In Electronic Components and Technology Conference (ECTC), 2012 IEEE 62nd (pp. 1695-1708). IEEE.

Lau, J., Solder Joint Reliability, Theory and Applications, Van Nostrand Reinhold, New York. 1991.

Li, R., Failure Analysis and Fatigue Prediction of Microprocessors Under Automotive Vibration Environments, Proceedings, International Systems Packaging Symposium, San Diego, CA. 1999.

Li, R., A Methodology for Fatigue Prediction of Electronic Components Under Random Vibration Load, Journal of Electronic Packaging, Volume 123, pp. 394–400, Dec. 2001.

Mason, S., Fatigue: a complex subject – some simple approximations, Society for Experimental Stress Analysis, Ohio 1964.

Miller, T., Schreier, H., Reu, P, High-speed DIC Data Analysis from a Shaking Camera System, Proceedings of

the SEM Conference, Springfield, Massachusetts, June 4-6, 2007.

Park, S., Shah, C., Kwak, J., Jang, C., Pitarresi, J., Transient Dynamic Simulation and Full-Field Test Validation for A Slim-PCB of Mobile Phone under Drop Impact, Proceedings of the 57th ECTC, Reno, Nevada, pp. 914-923, May 29 –June 1, 2007a.

Park, S., Reichman, A., Kwak, J., Chung, S., Whole Field Analysis of Polymer Film, Proceedings of the SEM Conference, Springfield, Massachusetts, June 4-6, 2007b.

Park, S., Al-Yafawi, A., Yu, D., Kwak, J., Lee, J., Goo, N., Influence of Fastening Methods on the Dynamic Response and Reliability Assessment of PCBS in Cellular Phones Under Free Drop, Proceedings of the ITherm, Intersociety Conference on Thermal and Thermo-mechanical Phenomena, Orlando, Florida, pp.876-882, May 28-31, 2008

Pitarresi, J.M., Modeling of Printed Circuit Cards Subject to Vibration, IEEE Proceedings of the Circuits and Systems Conference, New Orleans, LA, pp. 2104-2107, May 1990.

Pitarresi, J.M., et al, The Smeared Properties Approach to FE Vibration Modeling of Printed Circuit Cards, ASME Journal of Electronics Packaging, Volume 113, pp. 250-257, September 1991.

Pitarresi, J.M., Akanda, A., Random Vibration Response of a Surface Mounted Lead/Solder Joint, Proceedings of ASME International Electronics Packaging Conference, Volume 1, Binghamton, NY, pp. 207-217, Sept. 1993.

Qi, H., Ganesan, A., Osterman, M., Pecht, M., Accelerated testing and finite element analysis of PBGA under multiple environmental loadings, Proceedings of IEEE International Conference of Business Electronics Product Reliability, pp. 99–106, Apr. 2004.

Srinivasan, V., Radhakrishnan, S., Zhang, X., Subbarayan, G., Baughn, T., Nguyen, L., High Resolution Characterization of Materials Used In Packages through Digital Image Correlation, ASME InterPACK, July 17-22, 2005.

Steinberg, D., Vibration Analysis for Electronic Equipment, Wiley, New York, 1988.

Steinberg, D., Preventing Thermal Cycling and Vibration Failures in Electronic Equipment, Wiley, New York, 2001.

Tavernelli, J., Coffin, Jr. L., Experimental Support for Generalized Equation Predicting Low Cycle Fatigue, ASME Journal of Basic Engineering, Volume 84, pp. 533–541, Dec 1962.

Tee, T. Y. , Hun Shen Ng, Chwee Teck Lim, Eric Pek, Zhaowei Zhong, Board Level Drop Test and Simulation of TFBGA Packages for Telecommunication Applications, Proceedings of the 53rd ECTC, pp. 121-129, 2003.

Kumar, U., Dasgupta, A., An Incremental Damage Superposition Approach for Reliability of Electronic Interconnects Under Combined Acceleration Stresses, Presented at the ASME International Mechanical Engineering Congress & Exposition, Dallas, Texas, Nov. 1997-WA/EEP-13.

Upadhyayula, V.,K.,K., and Dasgupta, A., An Incremental Damage Superposition Approach for Reliability of Electronic Interconnects Under Combined Acceleration Stresses, ASME International Mechanical Engineering Congress & Exposition, Dallas, Texas, Nov., 1997.

Wong, E. H., Lim, C. T., Field, J. E., Tan, V. B. C., Shim, V. P.M., Lim, K. T., Seah, S. K. W., Tackling the Drop Impact Reliability of Electronic Packaging, ASME InterPAK, July 6 -11, Maui, pp. 1 – 9, 2003.

Wong, S., Malatkar, P., Rick, C., Kulkarni, V., Chin, I., 2007, Vibration Testing and Analysis of Ball Grid Array Package Solder Joints, Proceedings of the 57th ECTC, Reno, Nevada, pp. 914-923, May 29 –June 1, 2007a.

Wong, T., Kachatorian, A., Cohen, M., 1997, J-Lead Solder Thermal Fatigue Life Model, ASME International Mechanical Engineering Congress & Exposition, Dallas, Texas, Nov. 1997.

Yao QZ, Qu JM, Wu SX. Solder fatigue life in two chip scale packages, Proceedings of IEEE-IMAPS International Symposium on Microelectronics, pp. 563–570,1999.

Yu D., Al-Yafawi A., Nguyen T., Park S., Chung S., High-cycle fatigue life prediction for Pb-free BGA under random vibration loading, Microelectronics Reliability Vol. 51, pp. 649-656, 2011

Zhang, B., Liu, P., Ding, H., Cao, W., Modeling of board-level package by Finite Element Analysis and laser interferometer measurements, Microelectronics Reliability 50 (2010) 1021-1027

Zhao, Y., Basaran, C., Cartwright, A., Dishongh, T., An experimental observation of thermomechanical behavior of BGA solder joints by Moir'e Interferometry, Journal of Mechanical Behavior of Materials, Volume 10, No.3, pp. 135-146, 1999.

Zhou, P., Goodson, K. E., Sub-pixel Displacement and Deformation Gradient Measurement Using Digital Image- Speckle Correlation (DISC), Optical Engineering, Vol. 40, No. 8, pp 1613-1620, August 2001.